**Eidgenössische Technische Hochschule Zürich**

*Ecole polytechnique fédérale de Zurich*
*Politecnico federale di Zurigo*
*Swiss Federal Institute of Technology Zurich*

# A Robust Maxwell Formulation For All Frequencies

R. Hiptmair, F. Krämer[†] and J. Ostrowski[‡]

Research Report No. 2008-05
May 2008

Seminar für Angewandte Mathematik
Eidgenössische Technische Hochschule
CH-8092 Zürich
Switzerland

[†]University of Leipzig, Fakultät für Mathematik und Informatik, D-04103 Leipzig
[‡]ABB Switzerland Ltd., Corporate Research, CH-5405 Baden 5 Dättwil

# A Robust Maxwell Formulation For All Frequencies

R. Hiptmair, F. Krämer[†] and J. Ostrowski[‡]

Seminar für Angewandte Mathematik
Eidgenössische Technische Hochschule
CH-8092 Zürich
Switzerland

Research Report No. 2008-05 May 2008

**Abstract**

A novel unified method for the stable numerical solution of the time-harmonic Maxwells equations for any frequency is presented. The method is based on an extended $a - \varphi$ variational formulation of the full linear Maxwells equations. This formulation avoids stability problems in the stationary limit, where it reduces to the equations of electrostatics and magnetostatics. Both capacitive and inductive effects are taken into account in a robust fashion for all frequencies.

[†]University of Leipzig, Fakultät für Mathematik und Informatik, D-04103 Leipzig
[‡]ABB Switzerland Ltd., Corporate Research, CH-5405 Baden 5 Dättwil

## I. Introduction

We aim to devise a variational formulation of the full linear Maxwell's equations in frequency domain that remains stable when passing to the stationary limit. We consider the case, where field computation is confined to an artificially bounded domain $\Omega \subset \mathbb{R}^3$ of simple topolgy. The boundary $\partial\Omega$ is partitioned into three non-overlapping parts $\Gamma_0$, $\Gamma_1$, and $\Gamma_i$, where $\Gamma_0$ and $\Gamma_1$ must have positive distance, see Fig. 1 for a typical geometric situation. Inside $\Omega$ there is an ohmic conductor occupying the region $\Omega_c$.

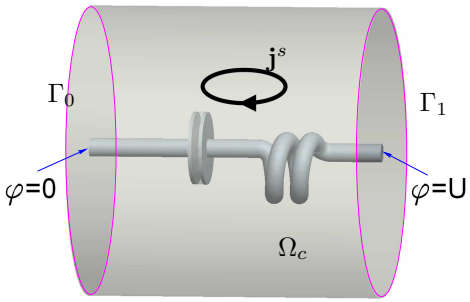


Fig. 1. RLC-arrangement: wire diameter 2.45 cm, diameter of capacitor plates 10 cm, distance of plates 1cm, distance of $\Gamma_0$ and $\Gamma_1$ is 40 cm. The resistance of the conductors represents a small R.

Voltage boundary conditions are imposed at $\Gamma_0$ and $\Gamma_1$, whereas ideal coils and space charges may be prescribed inside $\Omega$. The former are modelled by a solenoidal current $\mathbf{j}_0^s$, whereas the latter enter the model through a fictitious current $\mathbf{j}_1^s$ with $-\operatorname{div}\mathbf{j}_1^s = \rho^s$. For simplicity zero total charge is assumed, and both $\mathbf{j}_0^s$ and $\mathbf{j}_1^s$ have vanishing normal components on $\partial\Omega$. Summing up, in this setting both *inductive and capacitive effects matter*.

The Coulomb gauged $\mathbf{a}$-$\varphi$-formulation of Maxwell's equations supplemented with Ohm's law $\mathbf{j} = \sigma\mathbf{e} + \mathbf{j}_0^s$ inside $\Omega_c$ reads:

$$\begin{aligned} \mathbf{curl}\,\mu^{-1}\,\mathbf{curl}\,\mathbf{a} - (\omega^2\epsilon - i\omega\sigma)\mathbf{a} + \\ (i\omega\epsilon + \sigma)\,\mathbf{grad}\,\varphi &= \mathbf{j}^s\,, \quad (1)\\ \operatorname{div}(\epsilon i\omega\mathbf{a}) &= 0\,, \quad (2) \end{aligned}$$

where $\mathbf{j}^s = \mathbf{j}_0^s + i\omega\mathbf{j}_1^s$, and $\mu, \epsilon, \sigma$ stand for the uniformly positive material coefficients. Note that $\sigma \equiv 0$ outside $\Omega_C$. The PDEs (1)-(2) have to be supplied with the boundary conditions

$$\mathbf{a}\times\mathbf{n} = 0\,,\ \varphi = lU \quad \text{on } \Gamma_l,\ l = 0,1,\ U\in\mathbb{C}\,, \quad (3)$$

$$\left.\begin{aligned} \mathbf{curl}\,\mu^{-1}\,\mathbf{curl}\,\mathbf{a}\cdot\mathbf{n} = 0 \\ \mathbf{curl}_\Gamma\mathbf{a_t} = 0\,,\ \epsilon\mathbf{a}\cdot\mathbf{n} = 0 \end{aligned}\right\} \quad \text{on } \Gamma_i\,. \quad (4)$$

We wrote $\mathbf{n}$ for the exterior unit normal at $\partial\Omega$ and $\mathbf{a_t}$ for the tangential surface trace of the vector field $\mathbf{a}$. We also need to require that the vector potential does not contribute to the current, $\int_\tau \mathbf{a}\cdot\vec{\mathrm{d}}s = 0$ for any path $\tau$ connecting $\Gamma_0$ and $\Gamma_1$.

The variational form of (1)-(4) relies on the Sobolev spaces

$$V := \{\mathbf{v}\in\boldsymbol{H}(\mathbf{curl},\Omega)\colon \mathbf{curl}_\Gamma\mathbf{v_t} = 0 \text{ on } \partial\Omega,\ \int_\tau \mathbf{v}\cdot\vec{\mathrm{d}}s = 0\},$$
$$H(U) := \{\psi\in H^1(\Omega)\colon\ \psi_{|\Gamma_0} = 0,\ \psi_{|\Gamma_1} = U\}\,.$$

Integration by parts yields the weak form of (1)-(4): seek $\mathbf{a}\in V$, $\varphi\in H(U)$ such that

$$\begin{aligned} (\mu^{-1}\,\mathbf{curl}\,\mathbf{a}, \mathbf{curl}\,\mathbf{a}') - \omega^2(\epsilon\mathbf{a},\mathbf{a}') + i\omega(\sigma\mathbf{a},\mathbf{a}') \\ +((i\omega\epsilon+\sigma)\,\mathbf{grad}\,\varphi, \mathbf{a}') = (\mathbf{j}^s,\mathbf{a}')\,, \quad (5)\\ (\epsilon\mathbf{a}, \mathbf{grad}\,\varphi') = 0\,, \end{aligned}$$

for all $\mathbf{a}'\in V$, $\varphi'\in H(0)$ ($(\cdot,\cdot)\ \hat{=}\ L^2$ inner product). The mathematical theory of generalized saddle point problems [1] establishes that (5) has a unique solution for all $\omega > 0$.

## II. Low-frequency instability

It is well known that Gauss' law $\operatorname{div}(\epsilon\mathbf{e}) = \rho$ is contained in (5) for any $\omega > 0$, but becomes an independent equation in $\Omega_e := \Omega\setminus\overline{\Omega}_c$ in the stationary limit $\omega = 0$. This decoupling manifests itself as a loss of control of the scalar potential $\varphi$ in $\Omega_e$ in (5) as $\omega\to 0$. In mathematical terms, the norm of the solution operator for (5) will blow up as $\omega\to 0$; (5) lacks uniform stability as $\omega\to 0$, since the recovery of $\varphi$ becomes ill-posed. Eventually, even round-off errors will severely pollute any approximate solution for $\varphi$.

This is confirmed by numerical experiments, whose outcome is depicted in Fig. 2. We used curved tetrahedral meshes

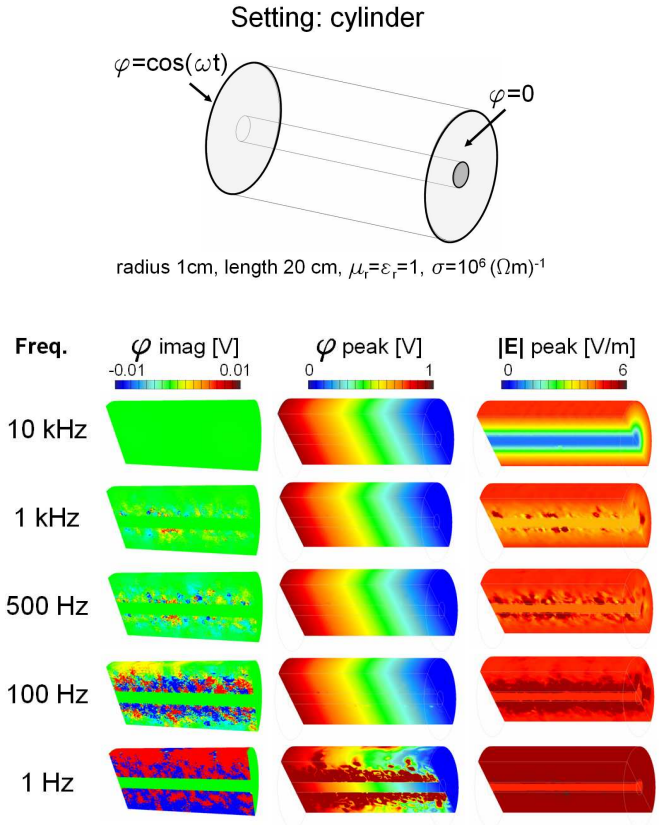


Fig. 2. 3D numerical experiments: solution of equation (5) on a simple test geometry for several frequencies on a tetrahedral mesh with 26000 nodes and 180000 edges resulting in 206000 complex unknowns.

throughout. Discretization employed (parametric) linear finite elements for the electric scalar potential and first order curved edge elements for the vector potential. A voltage difference

with complex amplitude 1 is imposed. The discretized problem is solved with the *direct sparse solver* Pardiso [2], integrated in the Intel Math Kernel Library 9.0. At 10 KHz this works well, a meaningful scalar potential $\varphi$ is obtained, and the skin effect is conspicuous. Below 1 kHz we lose control of $\varphi$ in the non-conducting region $\Omega_e$. This becomes especially visible in the imaginary part of the potential. As a result, the electric field is disturbed. Note that the potential, thus also the electric field, can accurately be recovered in the conducting domain even for small frequencies.

## III. Generating system approach

As an extremely simple model we study the variational problem

$$\vec{x} \in \mathbb{R}^2 : \quad \vec{x} \cdot \vec{y} = f(\vec{y}) \quad \forall \vec{y} \in \mathbb{R}^2 \,, \tag{6}$$

where $f$ is a linear functional on $\mathbb{R}^2$. The matrix representation of (6) with respect to the poorly conditioned basis $\mathfrak{B} := \{b_1 := \binom{1}{0}, b_2 := \binom{1}{\delta}\}$, $0 < \delta \ll 1$, of $\mathbb{R}^2$ is

$$\mathbf{A} = \begin{pmatrix} 1 & 1 \\ 1 & 1+\delta^2 \end{pmatrix} \,. \tag{7}$$

We may augment $\mathfrak{B}$ by the linearly dependent vector $b_3 := \binom{1}{-1} = (1+\frac{1}{\delta})b_1 - \frac{1}{\delta}b_2$, thus obtaining a *generating system* $\tilde{\mathfrak{B}} := \mathfrak{B} \cup \{b_3\}$. Here, $b_3$ was chosen such that $\tilde{\mathfrak{B}}$ contains a $\delta$-uniformly stable basis. When used to "discretize" (6), we obtain the *singular* matrix

$$\mathbf{C} := \begin{pmatrix} 1 & 1 & 1 \\ 1 & 1+\delta^2 & 1-\delta \\ 1 & 1-\delta & 2 \end{pmatrix} = \begin{pmatrix} \mathbf{A} & \mathbf{AG} \\ \mathbf{G}^T\mathbf{A} & \mathbf{G}^T\mathbf{AG} \end{pmatrix} \,, \tag{8}$$

with $\mathbf{G} = \binom{+1/\delta}{-1/\delta}$. The key observation is that most iterative solvers can well cope with singular matrices provided that the right hand sides of the linear systems are consistent [3]: crucial is the distribution of *non-zero* eigenvalues. Fig. 3 demonstrates this in the case of a simple Gauss-Seidel iteration: for small $\delta$ it converges much faster for the singular system than for the ill-conditioned. Of course, this striking difference is due to a judicious choice of $b_3$! It is worth noting that the very same augmentation idea accounts for the power of multigrid methods [4], [5] and has been used to enhance ILU-preconditioners in [6].

## IV. Stabilzed variational formulation

The generating systems approach can also be applied to variational problems set in function spaces, where it boils down to using *non-direct* decompositions of trial and test spaces. For (5) we may use the non-direct splitting

$$H(U) = H(U)' + H^1_e(\Omega) \,, \tag{9}$$

$$H^1_e(\Omega) := \left\{ \begin{array}{l} v \in H^1(\Omega) : \, v \equiv \text{const} \\ \text{on all connected components of } \Omega_c, \\ v_{|\Gamma_0} = 0, \, v_{|\Gamma_1} = 0 \,. \end{array} \right\} \,. \tag{10}$$

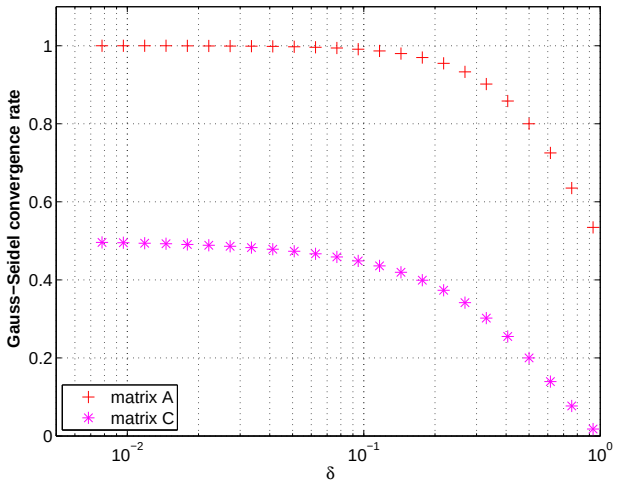


Fig. 3. Gauss-Seidel convergence rates (ratios of norms of subsequent residuals) for linear systems $\mathbf{A}\vec{x} = \vec{f}$ and $\mathbf{C}\vec{x} = \vec{f}$, the latter with consistent right hand side. Convergence rates determined by means of power iterations.

According to (9), in (5) we replace $\varphi$ with the sum $\varphi = \tilde{\varphi} + \psi$, $\tilde{\varphi} \in H(U)$, $\psi \in H^1_e(\Omega)$. The introduction of an extra unknown has to be balanced by an extra equation, which we obtain by testing the first equation of (5) with $\psi' \in H^1_e(\Omega)$:

$$\begin{aligned} -\omega^2(\epsilon\mathbf{a}, \mathbf{grad}\,\psi') + (i\omega\epsilon\,\mathbf{grad}(\tilde{\varphi}+\psi), \mathbf{grad}\,\psi') \\ = i\omega(\mathbf{j}^s_1, \mathbf{grad}\,\psi') \,, \end{aligned} \tag{11}$$

Note that $\mathbf{grad}\,\psi' \equiv 0$ inside $\Omega_C$. Equation (11) is redundant for any $\omega > 0$, but after dividing by $i\omega$ it represents Gauss' law in the non-conducting domain. This is exactly the information that is missing (5) in the stationary limit.

Thanks to the gauge condition, the first term of (11) evaluates to zero. Thus, we arrive at the following variational problem: seek $\mathbf{a} \in V$, $\tilde{\varphi} \in H(U)$, $\psi \in H^1_e(\Omega)$ such that for all $\mathbf{a} \in V$, $\tilde{\varphi}' \in H(0)$, $\psi' \in H^1_e(\Omega)$

$$\begin{aligned} (\mu^{-1}\,\mathbf{curl}\,\mathbf{a}, \mathbf{curl}\,\mathbf{a}') - \omega^2(\epsilon\mathbf{a}, \mathbf{a}') + i\omega(\sigma\mathbf{a}, \mathbf{a}') + \\ ((i\omega\epsilon+\sigma)\,\mathbf{grad}\,\tilde{\varphi}, \mathbf{a}') + i\omega(\epsilon\,\mathbf{grad}\,\psi, \mathbf{a}') &= (\mathbf{j}^s, \mathbf{a}') \,, \\ (\epsilon\,\mathbf{grad}\,\tilde{\varphi}, \mathbf{grad}\,\psi') &= 0 \,, \\ (\epsilon\,\mathbf{grad}\,\tilde{\varphi}, \mathbf{grad}\,\psi') + (\epsilon\,\mathbf{grad}\,\psi, \mathbf{grad}\,\psi') &= (\mathrm{div}\,\mathbf{j}^s_1, \psi') \,. \end{aligned} \tag{12}$$

If $(\mathbf{a}, \varphi)$ solves (5), then the same functions together with $\psi = 0$ will supply a solution of (12). Fittingly, in (12) the second equation arises from combining the first and the third. Both observations remain valid also after discretization by means of conforming finite elements, that is, in the case of edge element approximation for $\mathbf{a}$ and continuous piecewise linear element used for $\tilde{\varphi}$ and $\psi$. Consequently, the linear systems of equations arising from (12) will be square but *singular*, which is natural for the generating systems approach.

## V. Stationary limit

Setting $\omega = 0$ (stationary limit) in (12) perfectly decouples the system into the familiar and stable variational problems of stationary electromagnetism:

First, we recover the stationary currents boundary value problem inside the conductor and the electrostatic potential equation in $\Omega_e$ through testing the first equation with gradients, and using the second: find $\varphi \in H(U)$ with

$$(\sigma \,\mathbf{grad}\,\varphi, \mathbf{grad}\,\varphi')_{\Omega_c} = 0 \quad \forall \varphi' \in H(0)\ . \tag{13}$$

$$(\epsilon \,\mathbf{grad}\,\varphi, \mathbf{grad}\,\psi') = (\operatorname{div} \mathbf{j}_1^s, \psi') \quad \forall \psi' \in H_e^1(\Omega)\ . \tag{14}$$

Charge balance is hidden in the second variational equation, because integration by parts reveals $\int_{\partial\Omega_c} \epsilon \,\mathbf{grad}\,\varphi \cdot \mathbf{n}\,\mathrm{d}S = \int_{\partial\Omega_c} \mathbf{j}_1^s \cdot \mathbf{n}\,\mathrm{d}S$. The source term $\mathbf{j}_1^s$ enables us to fix the total charge of connected components of the conductor, which is another freedom in the stationary limit.

Second, the equations of magnetostatics emerge from the first and second equation of (12): with $\varphi$ from (13), (14), seek $\mathbf{a} \in V$ such that

$$\begin{aligned} (\mu^{-1} \,\mathbf{curl}\,\mathbf{a}, \mathbf{curl}\,\mathbf{a}') &= (\mathbf{j}^s, \mathbf{a}') - (\sigma \,\mathbf{grad}\,\varphi, \mathbf{a}')\ , \\ (\epsilon \mathbf{a}, \mathbf{grad}\,\varphi') &= 0\ , \end{aligned} \tag{15}$$

for all $\mathbf{a}' \in V$, $\varphi' \in H(0)$.

The bottom line is that the limit equations are perfectly well-posed, which bodes well for the behavior of iterative solvers when applied to a discretized version of (12): we can expect *robustness* with respect to small values of $\omega$.

## VI. Numerical experiments

The above numerical experiments, see Fig. 2, were repeated with the stabilized formulation (12). The same finite elements on the same mesh were used. The direct solver Pardiso [2] failed on the singular system resulting from (12). Conversely, an iterative preconditioned BiCGstab solver succeeded. A preliminary preconditioner was obtained by applying the direct solver to the discretized version of (12) after setting $\omega \leftarrow \max\{\omega, 1\,\mathrm{Hz}\}$, $\sigma(\boldsymbol{x}) \leftarrow \max\{\sigma(\boldsymbol{x}), 1\,\Omega\mathrm{m}^{-1}\}$. The finite element spaces remain unchanged. This removes the linear dependence of the equations. Nevertheless, this procedure provides a good approximation of (12), because of the continuity with respect to frequency and conductivity. We emphasize that this approach was chosen for testing purposes. For example, the direct solver can be replaced by an approximative LU decomposition based on $\mathcal{H}$-matrices, see [7], in future, more efficient implementations. Fig. 4 shows the results we obtained with the iterative solver. Using zero initial guess, independent of the frequency it took 3–5 BiCGstab iterations to reach a relative residual of $1.0 \cdot 10^{-14}$ (machine precision).

Fig. 4 highlights the improved stability of the new formulation: The electric potential, the electric field and the magnetic field are robustly computed for all frequencies, including the stationary case at 0 Hz. For this simple example a magneto-quasistatic approximation would also suffice (note the skin effect at 10 kHz). Obviously the stationary limit boils down to DC-conduction.

Conversely, the arrangement of Fig. 1 represents a situation that cannot be handled by any classical electro/magneto-quasistatic model. The stationary limit at 0 Hz is electrostatics, but coupled inductive and capacitive effects are present at all frequencies >0 Hz. The stability of the new formulation (12) together with an iterative preconditioned BiCGstab solver

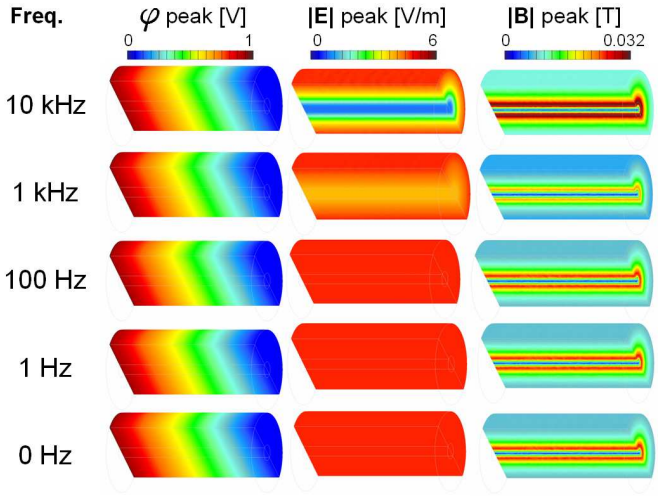


Fig. 4. 3D numerical experiments on the geometry of Fig. 2. Solution of equation (12) on a simple test geometry for several frequencies.

as above was tested for this geometry. Copper with material parameters $\sigma = 5.7 \cdot 10^7 (\Omega m)^{-1}$, $\mu_r = \epsilon_r = 1$ was used for the conductors. A complex voltage drop of $1V$ was imposed. Fig. 5 shows the results of the numerical experiments. The

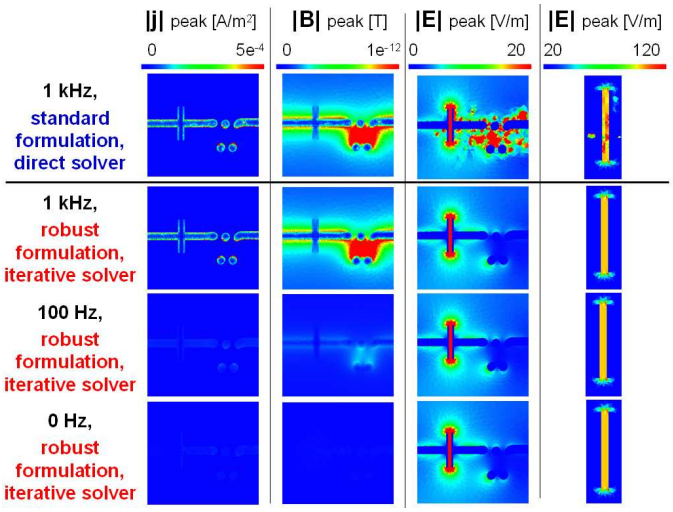


Fig. 5. Solutions of the equation (5) in the first row, and equation (12) in the other rows for a voltage of 1V. The mesh consists of 35000 Nodes and 240000 Edges, leading to 275000 complex unknowns.

same problems as described in Sec. II were found for the direct solution of equation (5) at 1 kHz: the electric field is disturbed in the nonconducting domain, especially in between the capacitor plates (right column). Yet, the iterative solver applied to the singular linear system of equations arising from (12) produced excellent results. Many essential electromagnetic effects are visible in Fig. 5: at 1kHz the current flows in a skin layer at the surface of the conductor. The magnetic field is repelled out of the conductors as well. The strongest magnetic field prevails inside the windings of the coil. A homogeneous electric field emerges between the capacitor plates (value = 100 V/m as expected) and it is very small inside the conductors.

The magnetic field and the current vanishes with decreasing frequency. A perfect electrostatic field is obtained at 0 Hz. For all different frequencies the preconditioned iterative solver converged within 3–5 steps to a relative residual of $1.0 \cdot 10^{-14}$.

We also investigated how well the computations yield the total current and the phase shift between voltage and current. Fig. 6 shows the results. The total current rises linearly for

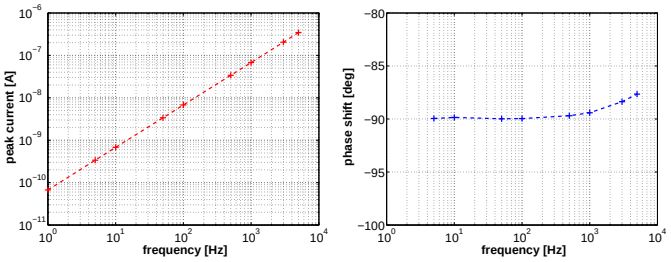


Fig. 6. results for total peak currents and phase shifts for the RLC-arrangement of Fig. 5. The conductivity was reduced to $1.0e^{-6}(\Omega m)^{-1}$ in order to avoid very small skin depths.

increasing frequency because the capacitor has to be loaded more often. Current and voltage are shifted about $-\pi/2$ for the complete 0-5 kHz frequency range, because the inductive impedance $i\omega L$ of the circuit is very small compared to the capacitive impedance $(i\omega C)^{-1}$.

Another example for coupled inductive and capacitive effects is shown in Fig. 7. The flat windings of the coil have a small distance and a strong electric field forms between them. The new formulation enables simulations for the entire range 50 Hz - 1 MHz of interesting frequencies.

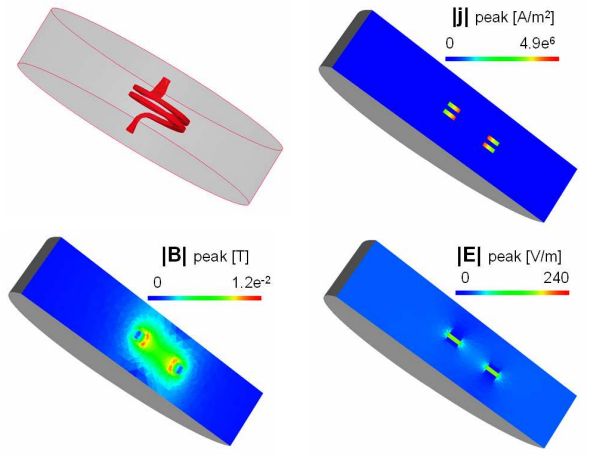


Fig. 7. Industrially relevant example arising in the context of electro-mechanical simulation of transformer windings: copper coil at 50Hz, applied test-voltage U=1V. Note the electric field between the windings

## VII. Conclusions

We have devised a generating system approach (12) to an $\mathbf{a} - \varphi$ formulation of Maxwell's equations in frequency domain. The new formulation, when discretized with conforming finite elements

- yields well posed and physically meaningful boundary value problems in the stationary limit $\omega \to 0$,
- allows the accurate simulation of combined capacitive and inductive effects in low frequency applications,
- is amenable to stable and fast iterative solution.

## References

[1] R. Nicolaides, "Existence, uniqueness and approximation for generalized saddle point problems", *SIAM J. Numer. Anal.*, vol. 19, no. 2, pp. 349–357, 1982.

[2] O. Schenk, Pardiso website, http://www.computational.unibas.ch/computer_science/people/schenk/software/.

[3] M. Hochbruck and C. Lubich, "Error analysis of Krylov methods in a nutshell", *SIAM J. Sci. Comput.*, vol. 19, pp. 695–701, 1998.

[4] M. Griebel, "Multilevel algorithms considered as iterative methods on semidefinite systems", *SIAM J. Sci. Stat. Comp.*, vol. 15, pp. 547–565, 1994.

[5] B. Weiss and O. Biro, "Multigrid for time-harmonic 3-d eddy-current analysis with edge elements", *IEEE Trans. Magnetics*, vol. 41, no. 5, pp. 1712–1715, 2005.

[6] H. Igarashi and T. Honma, "On convergence of iccg applied to finite-element equation for quasi-static fields", *IEEE Trans. Magnetics*, vol. 38, no. 2, pp. 565–568, 2002.

[7] M. Bebendorf, "Approximate inverse preconditioning of finite element discretizations of elliptic operators with nonsmooth coefficients", *SIAM J. Matrix Anal. Appl.*, vol. 27, no. 6, pp. 909–929, 2006.